Global and Planetary Change 196 (2021) 103364

Contents lists available at ScienceDirect

Global and Planetary Change

journal homepage: www.elsevier.com/locate/gloplacha

Effect of water on the rheology of the lithospheric mantle in young extensional basin systems as shown by xenoliths from the Carpathian-Pannonian region

Nóra Liptai [a,b,*], Thomas P. Lange [a,c,d], Levente Patkó [a,b,c], Zsanett Pintér [c,e], Márta Berkesi [a,c], László E. Aradi [c], Csaba Szabó [b,c], István J. Kovács [a,b]

[a] MTA CSFK Lendület Pannon LitH$_2$Oscope Research Group, Geodetic and Geophysical Institute, Research Centre for Astronomy and Earth Sciences, Sopron, Hungary
[b] Geodetic and Geophysical Institute, Research Centre for Astronomy and Earth Sciences, Sopron, Hungary
[c] Lithosphere Fluid Research Lab, Institute of Geography and Earth Sciences, Eötvös Loránd University, Budapest, Hungary
[d] Isotope Climatology and Environmental Research Centre, Institute for Nuclear Research, Debrecen, Hungary
[e] School of Earth, Atmosphere and Environment, Monash University, Melbourne, Australia

ARTICLE INFO

Keywords:
Lithospheric rheology
Mantle xenolith
Mantle water content
Carpathian-Pannonian region
Effective viscosity

ABSTRACT

Incorporation of hydrogen as structural hydroxyl (commonly referred to as water) in nominally anhydrous mantle minerals is known for the 'hydrolytic weakening' effect, which decreases the strength and electrical resistivity of the rock. Recent models have provided means of calculating rheological properties from geochemical data of upper mantle xenoliths. In the Carpathian-Pannonian region, upper mantle xenoliths can be found on the surface at five locations, both at marginal and central regions of the basin system. In this study we present a comprehensive overview of water contents in these xenoliths, including previously lacking data from two outcrops (Füzes-tó and Tihany) from the Bakony-Balaton Highland Volcanic Field for the first time. The Tihany xenoliths have significantly higher water contents (< 1–5, 116–353 and 327–1394 ppm in olivine, orthopyroxene and clinopyroxene, respectively) than the Füzes-tó xenoliths (0–2.7, 6.2–114 and 3.1–213 ppm in olivine, orthopyroxene and clinopyroxene, respectively). This can be explained with the older eruption age of their host basalt and greater depth of origin, as they likely represent an asthenospheric layer that became part of the lower lithosphere during thermal relaxation. In contrast, the Füzes-tó xenoliths represent a lot dryer mantle portion and are assumed to have been more affected by decompression-induced water loss resulting from decreased water activity during the extension.

In general, the marginal xenolith locations of the Carpathian-Pannonian region, associated to prior supra-subduction environment, contain more water than xenoliths from central locations (with the exception of Tihany locality) which were significantly affected by extension-related lithospheric thinning. To reveal the differences in rheology inferred from the different water contents, we calculated effective viscosities and electrical resistivities for the xenoliths of the Bakony-Balaton Highland and other locationss in the Carpathian-Pannonian region using previously published data for input. Based on the results, the central locations have higher effective viscosities ($1.4 \cdot 10^{20}$–$2.2 \cdot 10^{21}$ Pa s) and electrical resistivities (48–913 Ωm) compared to the marginal locations ($9.3 \cdot 10^{19}$–$6.8 \cdot 10^{20}$ Pa s and 36–182 Ωm, respectively), suggesting that the lithospheric mantle is more rigid in the former than in the latter areas. This may be a common feature for extensional basins, as the extension leads to the 'drying' of the upper mantle, whereas subduction zones keep hydrating their overlying mantle wedge. However, for more accurate estimations, other factors such as regional differences in strain rate or the potential presence of melts or fluids in the mantle need to be considered as well.

* Corresponding author at: MTA CSFK Lendület Pannon LitH$_2$Oscope Research Group, Mining and Geological Survey of Hungary, Budapest, Hungary.
E-mail address: liptai.nora@csfk.mta.hu (N. Liptai).

https://doi.org/10.1016/j.gloplacha.2020.103364
Received 15 May 2020; Received in revised form 20 October 2020; Accepted 26 October 2020
Available online 2 November 2020

1. Introduction

'Water' in the mantle can appear either as molecular H_2O (in fluids or melts) or as structurally bound hydroxyl (OH^-) in volatile-bearing or nominally anhydrous minerals (NAMs). The NAMs incorporate H^+ in atomic point defects (vacancies) bound to coordinating oxygens in their crystal structure (Martin and Donnay, 1972), and can contain up to hundreds of wt. ppm H_2O equivalent (Bell and Rossman, 1992), commonly referred to as water. The importance of water incorporated in NAMs of the mantle lies in the fact that it has a significant effect on physical properties, such as melting temperature (Green et al., 2010), electrical conductivity/resistivity (Selway et al., 2014), seismic wave attenuation (Aizawa et al., 2008) and deformation behavior (Mackwell et al., 1985; Hirth and Kohlstedt, 1996; Jung and Karato, 2001; Demouchy et al., 2012; Girard et al., 2013; Manthilake et al., 2013). Most studies focusing on the effect of water content on rheological properties (such as effective viscosity) and electrical conductivity/resistivity are experimental, and there is only a limited amount of publications aiming to examine this relationship on natural samples (Dixon et al., 2004; Li et al., 2008; Selway et al., 2014; Kovács et al., 2018). Furthermore, to date there are no data on how the link between water content and lithosphere rheology may behave in different tectonic environments.

For this purpose, we chose to examine mantle xenoliths from the Carpathian-Pannonian region (CPR), a young extensional basin system with a Neogene tectonic history. Upper mantle xenoliths were brought to the surface by late Miocene – Pleistocene alkali basalts in five locations, which include marginal areas associated to prior supra-subduction environment, and central areas distant from former subduction zones in their present tectonic position. Extensive research in the past decades resulted in a robust database on the petrographic, geochemical and deformational properties of these xenoliths, however, water content of NAMs are available from three volcanic fields: the Styrian Basin (Aradi et al., 2017), Nógrád-Gömör (Patkó et al., 2019) and Perşani Mountains (Falus et al., 2008; Lange et al., 2019).

In this paper, we present the water contents of 19 upper mantle xenoliths from two localities of the Bakony-Balaton Highland Volcanic Field (BBHVF), from where no such data has yet been published. Using the acquired water contents, we calculate effective viscosity and electrical resistivity for the lithospheric mantle beneath the BBHVF and the other three volcanic fields in the CPR from where such data are available. The main goal of this study is to provide a detailed comparison of water contents in various mantle portions of the CPR in different geodynamic positions and give insight on how it may affect the rheological properties in different tectonic areas of an extensional basin system.

2. Geological framework

The CPR, located in Central Europe, is generally understood as the broad region involving the Carpathians and their enclosed extensional basins, and is surrounded by the Bohemian Massif, the East European and Moesia Platforms, the Dinarides and the Alps. The CPR is considered to have formed with the juxtaposition of two microplates, the ALCAPA and Tisza-Dacia in the late Oligocene (Csontos et al., 1992; Horváth, 1993), following the extrusion and eastward migration of ALCAPA from the Alpine collision zone (Kázmér and Kovács, 1985; Ratschbacher et al., 1991). Simultaneously with the extrusion, the SW- then W-directed subduction of the Magura Ocean took place, and it terminated in continental collision during the early to middle Miocene with the N*E*- then E- migrating accretion wedge building up the Carpathians (e.g., Nemcok et al., 1998). During the middle Miocene, large-scale extension dominated the region, resulting from the combined effect of subduction rollback on the eastern margin of the CPR (Royden et al., 1982; Csontos, 1995), and gravitational instability resulting from thickened crust and lithospheric downwelling in the surrounding collision zones (Houseman and Gemmer, 2007). The extension and the accompanying asthenosphere updoming led to significant lithospheric thinning, which was the most extreme in the central areas of the Pannonian Basin (Royden et al., 1983; Horváth, 1993). From the late Miocene, tectonic inversion dominated the CPR resulting from the convergence and rotation of the Adria block in the direction of the East European platform (Horváth and Cloetingh, 1996; Bada et al., 2007).

From the early Miocene to Quaternary times, volcanic eruptions took place in the CPR with variable spatial distribution and chemical compositions ranging from calc-alkaline to Na- and K-alkali basaltic products (e.g., Szabó et al., 1992; Seghedi and Downes, 2011). The most widespread post-collisional intermediate calc-alkaline volcanism has been explained by the subduction and slab-breakoff along the Eastern Carpathians (e.g., Harangi, 2001). However, calc-alkaline volcanism in the northern Pannonian Basin, in the vicinity of the Western Carpathians were interpreted as the result of decompressional melting of the previously metasomatized mantle wedge and crustal contamination (Harangi, 2001; Seghedi et al., 2004). It was also proposed, in the lack of seismic evidence of a fully developed subduction under the Western Carpathians, that the geochemical characteristics were inherited from a subduction prior to the extrusion of the ALCAPA (Kovács and Szabó, 2008).

The Na-alkali basaltic volcanic activity took place from late Miocene to Pleistocene throughout the CPR, and brought upper mantle xenoliths to the surface at five locationss (e.g., Szabó et al., 2004), from west to east: Styrian Basin Volcanic Field (SBVF), Little Hungarian Plain Volcanic Field (LHPVF), Bakony-Balaton Highland Volcanic Field (BBHVF), Nógrád-Gömör Volcanic Field (NGVF), and Perşani Mountains Volcanic Field (PMVF) (Fig. 1). Among these, SBVF in the western and PMVF in the eastern margin, are located in the vicinity of former subduction zones. Beneath the SBVF, a downwelling structure inferred by seismic tomographic models (Lippitsch et al., 2003; Dando et al., 2011) was interpreted as the remnant of a detached European slab (Mitterbauer et al., 2011; Qorbani et al., 2015). Similarly, in the Carpathian Bend area near the PMVF, the remnant of a subducting slab was revealed by seismic tomography (e.g., Tondi et al., 2009; Ismail-Zadeh et al., 2012). However, the more central areas of the CPR, where the LHPVF and BBHVF are located, are far from subduction zones. The NGVF, located on the northern part of the CPR and close to the Western Carpathians, is also far from recent subduction zones, as no unequivocal sign for the subduction of the European plate was found under the Western Carpathians (Szafián and Horváth, 2006; Tašárová et al., 2009).

The lithospheric thickness is highly variable in the different locations of the CPR and depends on the applied method. Based on the map of Horváth et al. (2006), using a combination of S-wave velocities, P-wave delay times and magnetotelluric soundings, the thickness of the lithosphere is ~60–80 km under the LHPVF, BBHVF and NGVF, ~100 km under the SBVF and ~ 140 km under the PMVF. According to the 3D gravity modelling map of Tašárová et al. (2009), the base of the lithosphere is at ~70–90 km under the LHPVF, BBHVF and NGVF, and ~ 130 km under the SBVF. The latter is in sharp contrast with P and S receiver functions data published by Bianchi et al., (2014) which propose a depth of 60–80 km for the lithosphere-asthenosphere boundary beneath the SBVF. Combined 2D modelling of gravity, geoid, topography and surface heat flow data of Bielik et al., (2010) estimated lithospheric thicknesses of 80–100 km in the middle of the Pannonian Basin, ~100–120 km under the NGVF and SBVF, and 120–140 km under the PMVF. Although the exact depth values vary depending on the method, it can be stated that the lithosphere-asthenosphere boundary is significantly shallower in the central regions of the CPR compared to the western and eastern marginal areas. Note that while the NGVF can be argued to lie closer to the 'northern margin' of the Pannonian Basin, due to the thinner lithosphere and distance from subduction zones, its tectonic situation is more similar to the LHPVF and BBHVF, therefore will be hereafter referred to as one of the central locations.

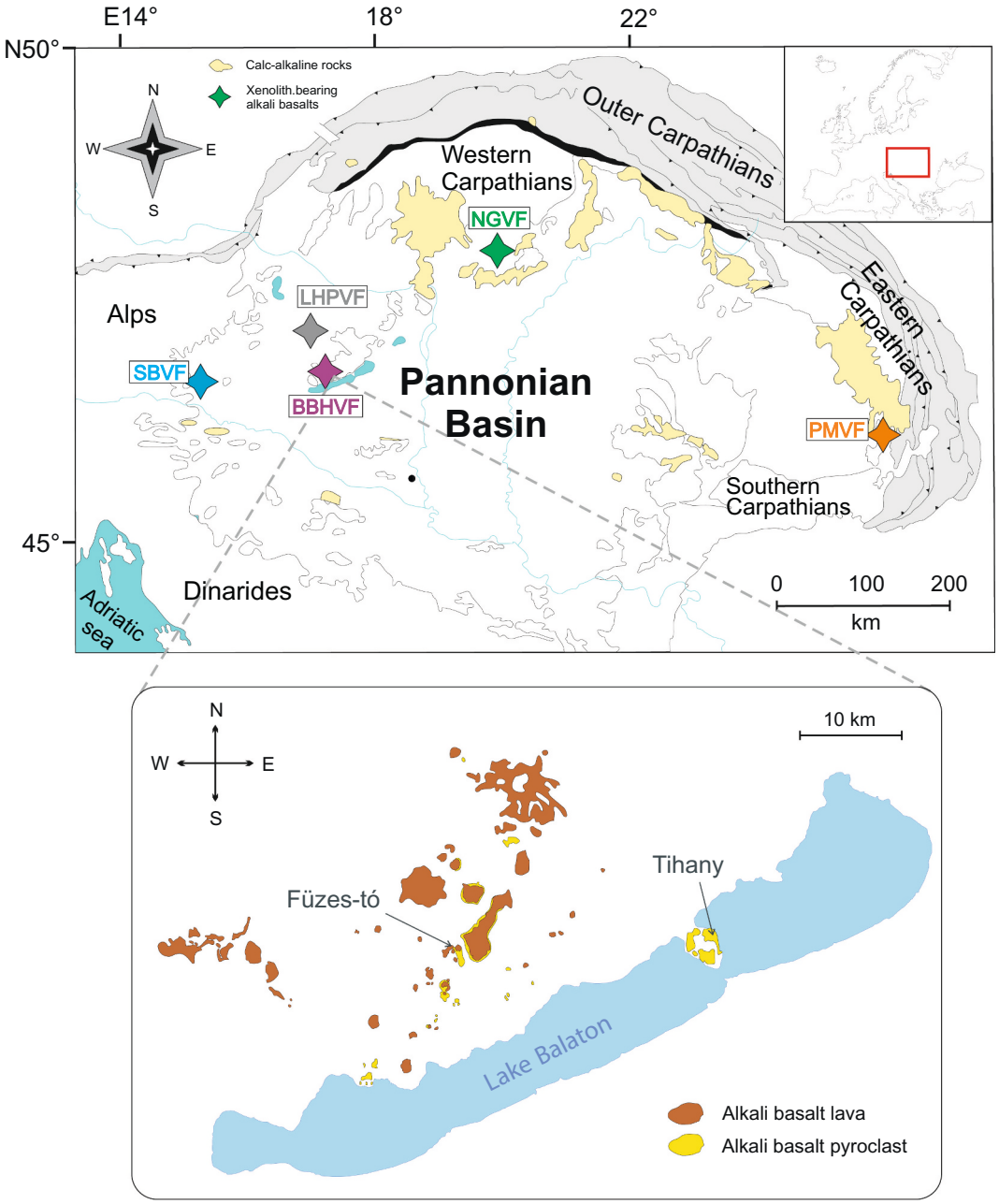

Fig. 1. Locations of the alkali basalt hosted upper mantle xenoliths in the Carpathian-Pannonian region (modified after Csontos and Nagymarosy, 1998), and distribution of alkali basaltic outcrops with sampling localities in the Bakony-Balaton Highland Volcanic Field (based on the Geological Map of Hungary 1:200000; L-33-XII-Veszprém after Jugovics, 1968, compiled by Harangi, 2001). Abbreviations: SBVF – Styrian Basin Volcanic Field, LHPVF – Little Hungarian Plain Volcanic Field, BBHVF – Bakony-Balaton Highland Volcanic Field, NGVF – Nógrád-Gömör Volcanic Field, PMVF – Perşani Mountains Volcanic Field.

3. Sampling and analytical methods

In the BBHVF, the alkali basaltic volcanism was active from around 8 to 2 Ma, based on K/Ar dating (Balogh et al., 1986; Pécskay et al., 1995; Balogh and Németh, 2005). Similar ages were revealed by $^{40}Ar/^{39}Ar$ geochronology carried out on a high number of basalt outcrops (Wijbrans et al., 2007). In this study, 6 xenoliths from the oldest locality, Tihany (7.96 ± 0.03 Ma) and 13 from the youngest one, Füzes-tó (2.61 ± 0.03 Ma) (Fig. 1) were examined. Tihany xenoliths, which are hosted in pyroclastite, were previously studied for their petrography and geochemistry (Berkesi, 2011; Berkesi et al., 2012). They are orthopyroxene-rich spinel lherzolites with coarse-grained (olivine grains sizing up to 2–4 mm) poikilitic texture, and fluid inclusions present in pyroxenes in several samples (Berkesi et al., 2012). Mg-numbers (Mg/[Mg + Fe]) of olivine, orthopyroxene and clinopyroxene vary between 0.90 and 0.91, 0.91–0.92, and 0.90–0.93, respectively, and calculated equilibrium temperatures range from 986 to 1148 °C (see Supplementary Table 2). Volcanic bombs of the Füzes-tó scoria cone host various xenocrysts and phenocrysts (Jankovics et al., 2009, 2012), however, peridotite xenoliths were only scarcely investigated before (Créon et al., 2017; Jankovics et al., 2012). The xenoliths of this study are dominantly lherzolite with a subordinate number of harzburgite and one olivine-orthopyroxenite (Table 1). Mg-numbers of olivine, orthopyroxene and clinopyroxene vary on a wider scale (0.89–0.92, 0.89–0.92 and 0.90–0.95, respectively, and equilibrium temperatures are between 825 and 1104 °C (Supplementary Table 2).

Water contents of the selected BBHVF xenoliths were obtained with Fourier-transform infrared spectroscopy (FTIR), using a Varian FTS

Table 1
Petrography and water content of the rock forming silicates of the studied BBHVF xenoliths. Rock types and mineral modal ratios of Tihany xenoliths are from Berkesi et al. (2012).

Sample	Rock type	ol (vol%)	opx (vol%)	cpx (vol%)	ol H_2O (ppm)	opx H_2O (ppm)	cpx H_2O (ppm)	Bulk H_2O (ppm)	$D^{cpx/opx}$
Füzes-tó									
FT082B	lhz	82	12	6	n.d.	6.9	6.4	1.2	0.9
FT001	lhz	63	30	5	0.4	20	72	9.8	3.6
FT0101	lhz	73	20	6	0.1	28	80	11	2.8
FT82A	lhz	75	19	6	n.d.	11	3.1	2.3	0.3
FT07	lhz	66	25	7	n.d.	16	61	8.3	3.8
FT08B	hzb	78	20	0	n.d.	6.2	20	1.2	3.2
FT042	lhz	70	25	8	2.8	74	213	37	2.9
FT0103	lhz	69	25	6	n.d.	30	67	12	2.2
FT0505	lhz	69	26	5	0.1	114	186	39	1.6
FT08B2	lhz	61	32	6	0.8	27	111	16	4.1
FTP5	lhz	54	27	18	0.3	47	108	32	2.3
FTP7	lhz	71	20	8	0.4	43	157	22	3.6
FTP8	ol-opx	39	60	<1	n.d.	13	n.d.	–	–
Tihany									
Tih0304	hzb	73	23	4	0.8	116	327	39	2.8
Tih0310	hzb	86	10	2	5.0	179	992	46	5.6
Tih0501	lhz	63	30	6	2.0	353	1394	183	4.0
Tih0506	hzb	72	25	3	2.7	153	714	58	4.7
Tih0507	hzb	55	42	3	0.3	117	661	66	5.7
Tih0509	lhz	59	26	12	1.1	128	424	87	3.3

n.d. - no absorption band detected.
lhz - lherzolite; hzb - harzburgite; ol-opx - olivine orthopyroxenite.
$D^{cpx/opx}$ - ratio of water content in clinopyroxene and orthopyroxene.

7000 FTIR spectrometer coupled to a Varian UMA-600 IR microscope at the Research Centre for Natural Sciences in Budapest. The analyses were carried out on double-polished thin sections with thicknesses ranging between 118 and 760 μm (Supplementary Table 1). For the measurements, a 'Globar' light source, KBr beam splitter and an MCT detector was used. Infrared spectra were collected in the spectral range of 4000–400 cm^{-1} with the use of a 100x100 μm aperture. Spectral resolution was 4 cm^{-1} and 256 scans were accumulated for both the background and the samples. The sample chamber and the interferometer were constantly flushed with compressed nitrogen during the analyses, with the purpose of reducing background resulting from atmospheric moisture and carbon dioxide.

The analyses were executed with unpolarized light, following the method of Sambridge et al. (2008) and Kovács et al. (2008), who showed that if the maximum linear unpolarized absorbance is less than 0.15, water content can be accurately determined averaging a few (at least 5) randomly oriented anisotropic crystals. However, fewer analyses are acceptable as well, as recently, Xia et al. (2013) proposed that in case of pyroxenes, even a single unpolarized measurement on an unoriented grain can achieve sufficiently accurate result. The water content is calculated using the total polarized absorbance (A_{tot}), which can be estimated as three times the average unpolarized integrated absorbance, and mineral-specific calibration factors. The (A_{tot}) was obtained using the OPUS software, following the data treatment described by Patkó et al. (2019). Integration ranges applied in this study are shown in Supplementary Table 1. Calibration factors were taken from Bell et al. (1995) for orthopyroxene (k_{opx} = 0.0674) and clinopyroxene (k_{cpx} = 0.14) and from Bell et al. (2003) for olivine (k_{ol} = 0.188). Water concentration values were normalized to 1 cm thickness. The thickness was measured with a Mitutoyo analogue micrometer in 5–6 spots on the sections and results were averaged. Based on prior experience, the cumulative uncertainty of this method (arising from background correction, choice of integration ranges, calibration factors and the statistical nature of the unpolarized analyses) does not exceed 30% (Kovács et al., 2008, 2012).

4. Results on water contents of BBHVF

Representative infrared spectra for Tihany and Füzes-tó xenoliths are presented on Fig. 2., and calculated water concentrations are contained in Table 1. For section thickness and additional spectral information (nr. of analyses, band positions, integration ranges and total integrated absorbances, see Supplementary Table 1).

4.1. Tihany

Xenoliths from the Tihany locality contain a significant amount of water, especially in pyroxenes (Table 1). Absorbance bands appear at 3572 and 3525 cm^{-1} in olivine in each sample, at ~3357 and ~ 3330 cm^{-1} in Tih0304, Tih0310, Tih0501 and Tih0506, and a wider band at ~3230 cm^{-1} in Tih0310 and weakly in Tih0304 and Tih0506. These band positions can be associated with Ti-clinohumite (Berry et al., 2005, 2007b; Walker et al., 2007), trivalent cation (Berry et al., 2007a; Blanchard et al., 2017) and Mg-substitution (Lemaire et al., 2004; Berry et al., 2005), respectively. Water concentrations in olivine range from <1 ppm up to a maximum of 5.0 ppm. Orthopyroxenes have absorbance bands at ~3600, 3520, 3420 and in two cases, at ~3320 cm^{-1}, and their water concentration range is between 116 and 353 ppm. Absorbance band positions in clinopyroxene appear at ~3640–3630, 3530–3520 and ~ 3450 cm^{-1}, and their calculated water concentration ranges from 327 to 1394 ppm. The infrared spectra of both orthopyroxene and clinopyroxene can be characterized by decreasing band intensity from the higher towards the lower wavenumbers (Fig. 2). Therefore, they can be labelled as type 1 according to the classification of Patkó et al. (2019), which is based on the ratio of absorbance for the different bands on pyroxene spectra.

4.2. Füzes-tó

The Füzes-tó xenoliths are generally more water-poor compared to the Tihany samples. There are no recognizable absorbance bands in olivine in 6 xenoliths (Table 1). Where there are, they appear at 3572 and 3525 cm^{-1}, indicating Ti-clinohumite substitution, and in FT042, FT0505 and FTP5 at ~3225 cm^{-1} indicating Mg-substitution. However, the calculation of water contents yielded values below 1 ppm except for xenolith FT042, which contains 2.7 ppm H_2O. Orthopyroxene absorbance bands appear at ~3588–3567, at ~3520 cm^{-1} and wider, less intense ones are sometimes present at ~3420–3410 and ~ 3315–3310

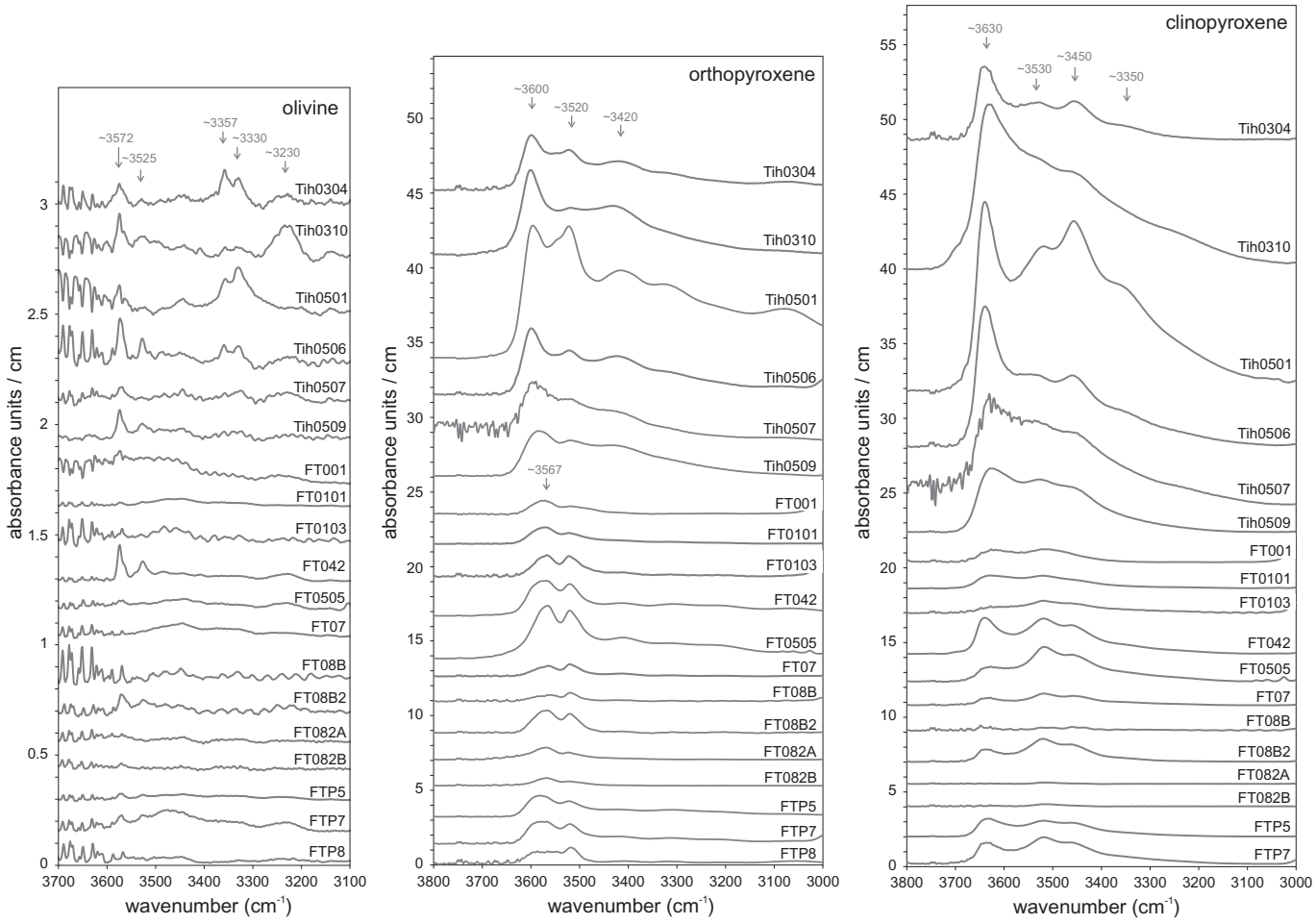

Fig. 2. Representative average unpolarized infrared spectra for olivine, orthopyroxene and clinopyroxene in the Füzes-tó and Tihany xenoliths. Absorbance units are normalized to 1 cm thickness.

cm^{-1}. The position range of the first band and the similar absorbance intensity of the first and second peak with a very subordinate third peak agrees well with type 2b orthopyroxene spectra described by Patkó et al. (2019). In clinopyroxene, absorbance bands are at ~3640–3630, 3520, and ~ 3460–3450 cm^{-1}. Among these peaks, either the first and second have similar intensities or the second one is the most intense. This classifies them as type 2a and 2b, respectively (Patkó et al., 2019). Calculated water concentrations of Füzes-tó pyroxenes range between 6.2 and 114 ppm (orthopyroxene) and 3.1–213 ppm (clinopyroxene). In two xenoliths (FT082A, FT082B), water contents of clinopyroxene are lower than those of orthopyroxene, which is rather uncommon and can be considered as extremely water-poor.

5. Water contents of xenoliths from other locations of the CPR

The two marginal volcanic fields, the SBVF and PMVF, have similar water concentration ranges in olivine (3.0–12.8 and 2.1–15.4 ppm), orthopyroxene (84–290 and 92–305 ppm) and clinopyroxene (190–674 and 186–632 ppm, respectively) (Falus et al., 2008; Aradi et al., 2017; Lange et al., 2019) (Fig. 3). They also fall within the water content range of off-craton peridotites reported worldwide (Peslier, 2010 and references therein). The water contents of the SBVF and PMVF were proposed to accurately represent the hydration state of the upper mantle beneath the volcanic fields, and the high concentrations were in both cases explained by their former supra-subduction environment, which was further supported by the high abundance of volatile-bearing minerals (mainly amphibole) (Falus et al., 2008; Aradi et al., 2017; Faccini et al., 2020), relatively to the central locations of the CPR. In both the NGVF and the BBHVF, only a few xenoliths were described to contain amphibole, usually as interstitial grains below 2 vol% or very rarely, appearing as vein (Embey-Isztin, 1976; Liptai et al., 2017; Bali et al., 2002, 2008; Szabó et al., 2009). These were interpreted as reaction products of either subduction-related melts/fluids (formed prior to the extension; Liptai et al., 2017) or hydrous basaltic melts rising up during the extension (e.g., Embey-Isztin, 1976; Szabó et al., 2009).

In the NGVF, the water content of NAMs in lherzolitic and wehrlitic xenoliths were studied separately (Patkó et al., 2019), as the latter group was shown to be metasomatic product of an interaction between a mafic melt and the lherzolitic wall rock (Patkó et al., 2020a). Therefore, for comparison with the rest of the CPR xenoliths, we only focus on the lherzolitic NGVF xenoliths. They have low water contents (maximum concentrations are 4.2, 98, and 481 ppm in olivine, orthopyroxene and clinopyroxene, respectively; Fig. 3), and in the majority of these xenoliths, olivines are completely dry. Patkó et al. (2019) proposed that the reason for these extremely low water contents may be the twofold. First, extension-related decompression led to decreased water activity, which means that the solubility of water in NAMs is reduced if other physico-chemical properties are unchanged. This results in re-equilibration under lower water activity, leading to reduced water contents. Second, further hydrogen loss occurred on the surface following the host basalt eruption due to slow cooling, which is supported by the better preservation of water content in xenoliths hosted by fast-cooling pyroclastic rocks.

The ratio of water content in clinopyroxene and orthopyroxene is a

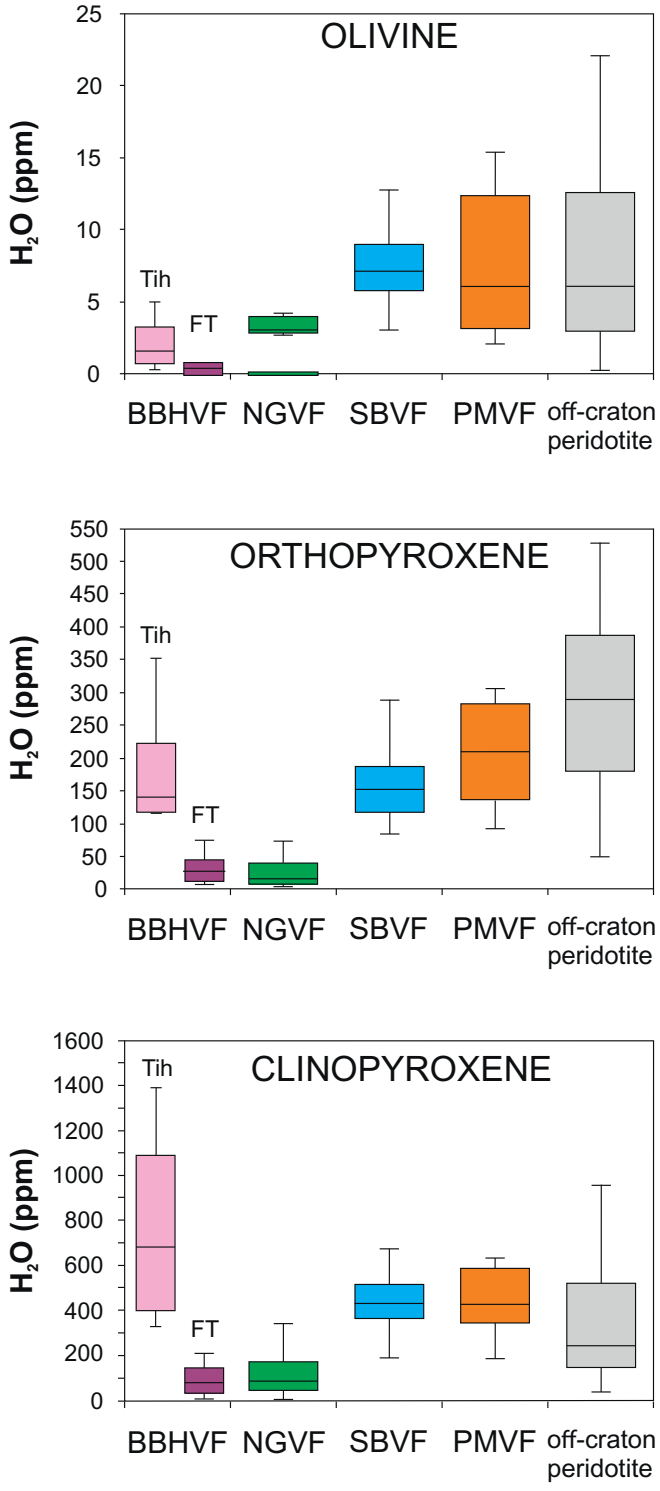

Fig. 3. Ranges of water content in olivine, orthopyroxene and clinopyroxene of xenoliths from different locations in the CPR and from off-craton peridotites worldwide for comparison. Abbreviations are the same as in Fig. 1. Data sources: SBVF - Aradi et al. (2017); PMVF - Falus et al. (2008), Lange et al. (2019); NGVF - Patkó et al. (2019); off-craton peridotites - Karato (2010) and references therein.

good indicator for water loss. Based on review works involving a great number of mantle xenoliths (Demouchy et al., 2017; Peslier et al., 2017; Xia et al., 2019), the partition coefficient ($D^{cpx/opx}$) varies between 1.5 and 3.5, which is hence considered as 'normal' for natural peridotites and implies higher water activity. Xenoliths of the SBVF and PMVF fall within this range (Fig. 4), whereas most of the NGVF xenoliths plot outside this field, showing higher $D^{cpx/opx}$ values. This was interpreted as a sign of hydrogen loss (Patkó et al., 2019), which is faster and more detectable in orthopyroxene than in clinopyroxene (Tian et al., 2017).

6. Discussion

6.1. Interpretation of water contents in xenoliths of the BBHVF

There is a significant difference between the water contents of Tihany and Füzes-tó xenoliths, not only in the calculated concentrations, but in the character of their infrared spectra as well. The xenoliths from Tihany show consequently higher water concentrations (Fig. 3, Table 1), whereas those from Füzes-tó are a lot 'dryer', as displayed by considerably lower absorbance intensities in their spectra (Fig. 2). Furthermore, both orthopyroxene and clinopyroxene spectra of the Füzes-tó xenoliths can be classified as type 2 (Patkó et al., 2019), i.e., the absorbance peak at the highest wavenumber is not the one with the greatest intensity. Such spectra are not common worldwide and were explained as a result of water loss in the mantle due to tectonic processes, namely extension-related decompression and the accompanying decrease in water activity in case of the NGVF (Patkó et al., 2019). We suggest that the water-poor nature of the Füzes-tó xenoliths can be explained with the same process, meaning it suffered hydrogen loss as a consequence of decreased water activity during the extension. Note that the xenoliths were retrieved from scoria cones, which go through relatively rapid cooling, therefore the slow cooling at higher temperature is less likely to account for the water loss. Nevertheless, it cannot be excluded either, as the water content of olivines is very low compared to what it should be based on the clinopyroxenes within the same xenoliths

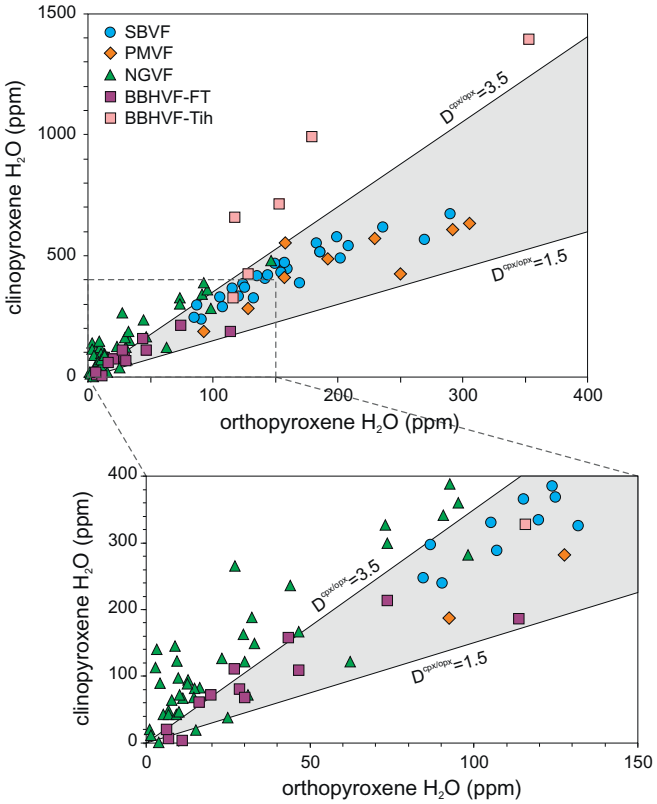

Fig. 4. Partitioning of water in orthopyroxene vs. clinopyroxene in the xenoliths of the CPR. Trendlines defining the 'normal' range ($D^{cpx/opx}$ = 1.5–3.5) are from Xia et al. (2019). Sources of data for the xenoliths: SBVF - Aradi et al. (2017); PMVF - Falus et al. (2008), Lange et al. (2019); NGVF - Patkó et al. (2019).

(Table 1), if we consider the general observation that $D^{cpx/ol} = \sim 10$ (e.g., Xia et al., 2019). This is also the case for the Tihany xenoliths, where the contrast between olivine and pyroxenes is even more evident.

The high water content of pyroxenes in Tihany xenoliths suggests that they were not, or only minimally affected by decompression-induced water loss. One possible explanation could be the difference in the eruption ages of the host basalt of the two localities, as the Tihany basalts are significantly older (7.96 Ma) than the Füzes-tó basalts (2.61 Ma) (Wijbrans et al., 2007). This would suggest that the water loss mainly occurred during this time period. Furthermore, the spatial distance, even though it is relatively small (~25 km; Fig. 1), may have a role in the compositional differences. However, there is another factor that needs to be taken into account. The averagely higher equilibrium temperatures of the Tihany xenoliths (986–1148 °C; Supplementary Table 2) suggest a greater depth of origin compared to the Füzes-tó ones (825–1104 °C; Supplementary Table 2). Based on the crystal preferred orientation patterns of BBHVF xenoliths, Kovács et al., 2012a proposed that following the peak period of the Miocene extension, the uppermost layer of the updomed asthenosphere (~40–60 km depth) became part of the lower lithosphere during the tectonic inversion and thermal relaxation. Since, compared to the age of Füzes-tó, the eruption time of the Tihany basalts occurred not long after the cessation of the *syn*-rift phase, which is estimated at ~13 Ma in the southwestern and ~ 8 Ma in the eastern Pannonian Basin (Balázs et al., 2016 and references therein), the xenoliths may have been sampled from the asthenosphere, or, more likely, a newly accreted lithospheric mantle portion.

The high water content of the Tihany xenoliths (even compared to the marginal locations of the CPR) could be in agreement with the lack of pargasite. Under circumstances characteristic for the upper mantle, pargasite, which is the main water-bearing mineral, is stable up to ~1050–1150 °C (~ 90–100 km) depending on the fertility (Green et al., 2010; Wallace and Green, 1991). In greater depths, where pargasite is no longer stable, the activity of water increases and excess water can be incorporated into NAMs (and fluids/melts), which results in a significant change in rheology. Kovács et al., n.d., 2017 proposed that in areas with thin lithosphere, such as the central part of the Pannonian Basin, the upper limit of pargasite stability could coincidence with the lithosphere-asthenosphere boundary. The high equilibrium temperatures of the Tihany xenoliths and their depleted character (Berkesi, 2011) suggest that in the mantle portion they represent, pargasite may not have been stable. It is also supported by the fact that previous studies did not find any pargasite in the Tihany xenoliths (Berkesi et al., 2012), whereas it is present in xenoliths from other BBHVF localities with younger eruption ages and lower equilibrium temperatures (Embey-Isztin, 1976; Bali et al., 2002; Créon et al., 2017; Szabó et al., 2009). However, the temperature range itself in the Tihany xenoliths does not prove asthenospheric origin, so we consider it more likely that their origin is in the lower lithospheric mantle.

The ratio of water contents in clinopyroxene and orthopyroxene in the Tihany xenoliths is higher than the empirically determined range characteristic for peridotites worldwide which show equilibrium in the distribution of water between NAMs (Fig. 4). This may indicate that water loss could have started to some extent in orthopyroxenes, which also favors the option that the xenoliths were transported to the surface after the onset of the post-extensional thermal relaxation, when the uppermost asthenospheric layer is suggested to have become part of the lithosphere (e.g., Kovács et al., 2012a). On the other hand, the Füzes-tó xenoliths fall mostly within or only slightly out of the $D^{cpx/opx} = 1.5–3.5$ range (Fig. 4). A possible explanation for this discrepancy could be that the Füzes-tó xenoliths were affected by decompression-related water loss to a greater extent (likely due to their longer residence time in the upper mantle after the paroxysm of the extension), and some of them could have re-equilibrated under the changed conditions. Because of the different diffusivity of H^+ in orthopyroxene and clinopyroxene (e.g., Stalder and Skogby, 2003; Ferriss et al., 2016; Tian et al., 2017), the lack of equilibrium could result in an increased $D^{cpx/opx}$. In this interpretation, the Tihany xenoliths represent a mantle portion in a transitional stage during the re-equilibration process and decreasing water activity.

6.2. Determination of rheological properties

Water incorporated in mantle silicates has been shown to actively affect physical properties, for example, it reduces effective viscosity. This effect is called hydrolytic weakening (e.g., Brodholt and Refson, 2000; Mei and Kohlstedt, 2000; Girard et al., 2013; Tielke et al., 2017). Effective viscosity and electrical resistivity, which is also strongly influenced by water content, were previously determined for part of the xenolith set of the CPR (Kovács et al., 2018; Lange et al., 2019), however, data from the BBHVF and a detailed comparative description of the different localities was not yet carried out. We calculated these two parameters for the xenoliths of the BBHVF and other CPR volcanic fields where they were not available previously, using data on xenoliths from previous studies (Falus et al., 2008; Aradi et al., 2017; Lange et al., 2019; Patkó et al., 2019). Effective viscosities and electrical resistivities for the PMVF xenoliths (Kovács et al., 2018) were re-calculated with equilibrium temperatures uniformly using the Ca-in-opx thermometer (Nimis and Grütter, 2010). Electrical resistivities of the NGVF xenoliths were calculated by Patkó et al., n.d., following the same method (see details below).

As discussed earlier, olivines have likely lost some part of their original water contents during their ascent, and/or the following cooling on the surface. To estimate the original water contents of olivine, we used the empirical equilibrium partition coefficient of water between clinopyroxene and olivine ($D^{cpx/ol} = \sim 10$) (e.g., Xia et al., 2019). The validity of this estimation is based on the approach that the diffusion speed of hydrogen is significantly lower in clinopyroxene than in olivine (Ferriss et al., 2016; Lloyd et al., 2016), and thus clinopyroxene is more likely to retain its original water content after being transported to the surface, even if water loss occurred in orthopyroxene and olivine.

6.2.1. Effective viscosity

Although effective viscosity can be calculated for multiple deformation mechanisms, we assumed dislocation creep since it is widely accepted to be the dominant deformation mechanism in the upper mantle based on the average stress and grain size (e.g., Karato, 2010 and references therein). Strong crystal preferred orientation of the CPR xenoliths where such data are available (Falus et al., 2008; Kovács et al., 2012a; Aradi et al., 2017; Liptai et al., 2019) further support deformation by dislocation creep, whereas diffusion creep is rather expected to occur only locally (e.g., in shear zones; Warren and Hirth, 2006).

When calculating effective viscosities, we followed Eq. 2 of Dixon et al. (2004), with material constants for wet dislocation at constant C_{OH} (Hirth and Kohlstedt, 2003). This model is based on olivine only, as being the dominant mineral in the upper mantle, its water content has a major control on the rheology. Temperature values were calculated using the Ca-in-opx thermometer of Brey and Köhler (1990) modified by Nimis and Grütter (2010) for the BBHVF and PMVF, where it was not published before. Pressures were estimated from equilibrium temperatures uniformly using the alkali province geotherm by Jones et al. (1983). We performed the calculations both with a strain rate of 10^{-14} and 10^{-15} s^{-1} following the estimation of Falus et al. (2008). The resulting effective viscosities for each xenolith of the BBHVF and the rest of the CPR are contained in Supplementary Table 2. Xenoliths which had lower water contents in clinopyroxene than in orthopyroxene (FT82A, FT082B; Table 1) were omitted for the calculations because they are assumed to not represent equilibrium mantle conditions.

Using a strain rate of 10^{-14} s^{-1}, effective viscosities of xenoliths from the marginal locations show a uniform distribution, ranging from $9.3 \cdot 10^{19}$ to $6.6 \cdot 10^{20}$ Pa s in the SBVF and from $1.2 \cdot 10^{20}$ to $6.8 \cdot 10^{20}$ Pa s in the PMVF (Fig. 5a). However, while having roughly the same equilibrium temperature range, the NGVF and BBHVF–Füzes-tó

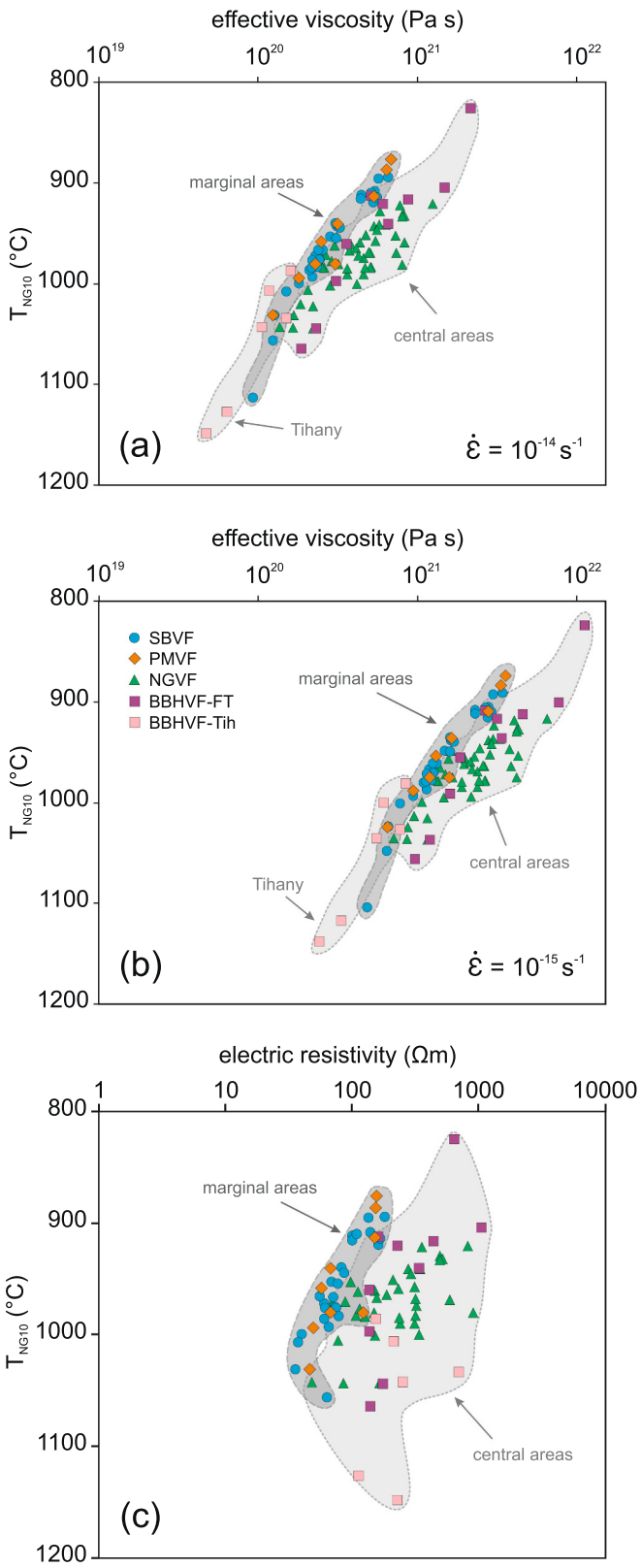

Fig. 5. a, b – Calculated effective viscosities of CPR xenoliths in the function of temperature, using strain rates ($\dot{\varepsilon}$) of 10^{14} and 10^{15} s^{-1}, respectively. c – Calculated electric resistivities of the CPR xenoliths. T_{NG10} – equilibrium temperature calculated using the Ca-in-opx thermometer of Brey and Köhler (1990) modified by Nimis and Grütter (2010). Electrical resistivities of the NGVF are taken from Patkó et al. (this issue).

xenoliths have higher effective viscosities ($1.4 \cdot 10^{20}$–$1.3 \cdot 10^{21}$ and $1.9 \cdot 10^{20}$–$2.2 \cdot 10^{21}$ Pa s, respectively). Note that the overlap in the effective viscosity values is due to their decrease with depth and increasing temperature (Fig. 5a). For the same temperatures, however, there is approximately a factor of five difference between xenoliths of the marginal and the central locations, which is a direct consequence of the differences in water content. Interestingly, the Tihany xenoliths are more similar to the marginal locations regarding their effective viscosities, which can be explained by their higher water contents, resulting from the lack of pargasite in them as discussed earlier.

It must be noted that uncertainty may rise from the used strain rate. In the literature, there are only estimates for the strain rate in the CPR. Falus et al. (2008) calculated strain rates between 10^{-14} and 10^{-15} s^{-1} for the upper mantle below 40 km in the PMVF. Numerical modelling by Balázs et al. (2018) predicted maximum strain rates of 10^{-14} s^{-1} along reactivating lithospheric-scale faults during extension. Jarosinski et al. (2011) suggested strain rates of 10^{-15}–10^{-16} s^{-1} for the central and marginal parts of the Pannonian Basin during tectonic inversion. Other studies (e.g., Horváth and Cloetingh, 1996; Lenkey et al., 2002) generally accept a value of 10^{-15} s^{-1} for bulk lithospheric strain rate in the CPR. Although we lack exact values for the xenolith locations, there may be some differences in the strain rate, which could also affect the effective viscosities. Calculating the effective viscosities using a strain rate of 10^{-15} s^{-1} results in approximately half a magnitude higher values (Fig. 5b), which suggests that strain rate may have a stronger effect on the effective viscosities than water content, provided that such high differences exist within the CPR. Nevertheless, assuming more or less similar strain rates for the different xenolith locations, it can be concluded that the marginal and more water-rich areas are less viscous than the central, dryer locations.

6.2.2. *Electrical resistivity*

Numerous experimental studies revealed that olivine and pyroxenes act as semi-conductors in mantle conditions, and their conductivity is strongly influenced by their water content as a function of pressure and temperature (e.g., Wang et al., 2006; Yoshino et al., 2009; Poe et al., 2010; Novella et al., 2017). Most of the experimental models take only olivine into account as the most abundant constituent of the upper mantle; however, there are several models which include pyroxenes and geochemical composition (Fe proportion with respect to Mg) as well (Jones et al., 2009, 2012; Fullea, 2017), as they also affect the bulk resistivity/conductivity of the lithospheric mantle.

We used the model of Fullea (2017) which calculates conductivity and resistivity for the individual minerals and for bulk rock, taking into account the modal proportion, water content and Fe proportion (Fe/[Mg + Fe] in molar concentrations) of olivine, orthopyroxene and clinopyroxene. The conductivity of a mineral consists of contributions from (1) small polarons depending on Fe content, (2) ionic diffusion, and (3) proton conduction resulting from the diffusion of H^+ in the crystal structure (see Eq. 4 of Fullea, 2017). Calculations were carried out following the same parameterization as described by Kovács et al. (2018). The excel sheet modified after Kovács et al. (2018) is available as Supplementary Table 3. Again, xenoliths FT082A and FT082B which have $D^{cpx/opx} < 1$ (Table 1), were omitted from the calculations for reasons mentioned above.

In general, the distribution of electrical resistivities show a decrease with temperature (Fig. 5c), and hence, depth, which is in agreement with previous findings stating that NAMs of the mantle become more conductive towards higher temperatures (e.g., Jones et al., 2012; Selway, 2014). Similarly to effective viscosities, electrical resistivity values are different for the marginal and the central xenolith locations. In the SBVF and PMVF, resistivities range in a relatively narrow range (36–182 Ωm and 45–157 Ωm, respectively). In comparison, the central locations have not only higher resistivities but also higher variability in the values (Fig. 5c). NGVF xenoliths range between 48 and 913 Ωm (Patkó et al., submitted), and BBHVF–Füzes-tó xenoliths between 138 and 644 Ωm.

The variability in these locations is resulting from the variable water contents, which can reach up to one magnitude of difference in clinopyroxene, whereas in the marginal locations, clinopyroxene water contents stay well within the same magnitude. In contrast with effective viscosities, Tihany xenoliths show resistivities which are high (113–703 Ωm) and more similar to the other central part xenoliths, despite the high water contents (Table 1, Fig. 5c). This can be explained by their relatively low clinopyroxene and high orthopyroxene modal proportion (Berkesi et al., 2012), as well as their depleted geochemical character (Mg-numbers are at or above 91 in all three silicate constituents; Berkesi, 2011). These features were interpreted to be the result of a reaction with a boninitic melt which led to the increase of orthopyroxene at the expense of olivine while leaving clinopyroxenes intact (Berkesi, 2011), as recognized previously in a xenolith from another BBHVF locality (Bali et al., 2007). This boninitic melt was proposed to be related to a subduction preceding the extrusion of the ALCAPA and formation of the Pannonian Basin (Bali et al., 2007; Kovács and Szabó, 2008; Berkesi, 2011). Such a metasomatic reaction could even account for the high $D^{cpx/opx}$ in the Tihany xenoliths, as the newly formed orthopyroxenes may contain less water compared to what would be in equilibrium with clinopyroxenes.

The advantage of electrical resistivity/conductivity calculations is that they can be compared and co-evaluated with deep magnetotelluric (MT) soundings (e.g., Selway et al., 2014) where they are available. In the Pannonian Basin, Ádám et al. (2017) reported resistivities of ~20–40 Ωm from deep MT sounding curves for the depth range represented by the xenoliths (40–50 km), which is somewhat lower than the calculated values. However, local deep MT profiles for the xenolith locations are only available in the NGVF, where resistivities are in good agreement with values determined in this study (few tens - few hundreds Ωm; Patkó et al., submitted), except for a low resistivity (<10 Ωm) portion under the central part, which was recognized to be related to the wehrlite-forming metasomatic process (Patkó et al., 2020a).

6.3. Tectonic implications

The results of the rheological calculations indicate that the upper mantle of the CPR has lower effective viscosities and electrical resistivities in the marginal areas than in the central ones. This is a consequence of the different water content in the studied mantle portions, resulting from their different tectonic environment. We propose that such difference may exist in the rheology of continental rift areas surrounded by or adjacent to active or former subduction zones and associated orogens of varying age, which are characteristic for the Mediterranean region (e.g., Faccenna et al., 2014), provided that there are no major differences in the strain rate. In fact, rheological heterogeneity is suggested to arise directly from subduction rollback driven extension, as the lithospheric thinning and updoming of underlying asthenosphere leads to a decrease in pressure. As discussed before, decompression causes a decrease in the activity of water, therefore this will result in re-equilibration of water contents in NAMs (Patkó et al., 2019) and the lithosphere becoming more rigid. This may imply that the extending lithospheric mantle achieves new equilibrium under lower water activities and therefore resists more and more to further extensional forces.

The presence of pargasite at lower temperatures can further contribute to the strengthening of the ambient upper mantle by incorporating water and thus lowering water activity (Kovács et al., 2017), which applies especially to the Tihany xenoliths. However, it must be noted that water is likely not the only factor that has a significant impact on the viscosity of the upper mantle, as a change of as much as one magnitude in the strain rate can have a considerable effect as well (Fig. 5a, b). In summary, water content and strain rate appear to be the two major controller of rheology in the lithospheric mantle.

6.4. Potential effects of fluids or partial melts in the mantle

Besides strain rate, a further source of uncertainty may be the potential presence of melts and fluids in the upper mantle, as the models applied in this study (Dixon et al., 2004; Fullea, 2017) are constructed for solid phases only. It was shown by experimental studies that basaltic melts can significantly increase electrical conductivity (Ni et al., 2011; Miller et al., 2015) even in a small fraction (as low as 0.5%) by forming an interconnected network along grain boundaries (Laumonier et al., 2017). It is not uncommon for small amounts of melts to be present in the upper mantle. In areas controlled by former subduction environment, presence of slab-derived fluids and melts is supported by the well-hydrated state of the upper mantle (i.e., higher water content of NAMs and abundance of volatile-bearing minerals), as described for the SBVF (Aradi et al., 2017) and the PMVF (Falus et al., 2008; Lange et al., 2019), however, their interconnectivity is questionable. Although melt and fluid inclusions are also abundant in CPR xenoliths (Szabó et al., 1996, 2009; Berkesi et al., 2012), they are not interconnected either, and therefore likely have negligible effect on the electrical conductivity.

Partial melts, nevertheless, could still be present in the asthenosphere beneath the central part of the CPR. Kovács et al. (2020) recently suggested that the asthenosphere appears to be 'wet' due to prior subductions or hydrous upwellings from the mantle transition zone. Their proposition, suggesting that basaltic melts were squeezed from the asthenosphere towards the surface by compressional forces during the tectonic inversion, is also in agreement with the potential presence of partial melts. These melts can explain ongoing metasomatic processes in the lithospheric mantle, as it was proposed for the NGVF by Patkó et al. (this issue). This interaction forming wehrlites out of lherzolites was revealed previously with detailed geochemical studies on the xenoliths (Liptai et al., 2017; Patkó et al., 2020a). Calculations of Patkó et al. (submitted) verified that the wehrlitized (i.e., clinopyroxene-enriched) mantle portion alone could not account for the low resistivities (<10 Ωm) revealed by deep MT soundings. Instead, the contribution of ~2–3 vol% of interconnected melt is required to achieve the observed low resistivities. Furthermore, a recent micro-CT study by Patkó et al., 2020b found interconnected glass in NGVF wehrlite xenoliths, which was proposed to represent remnant of the metasomatic agent (basaltic melt) at upper mantle depths. In conclusion, the potential presence of melts in the upper mantle cannot be excluded for the CPR either, and needs to be taken into account when estimating electrical resistivity. Moreover, recent studies (Sifré et al., 2014) reported the significance of volatile composition of the basaltic melts, namely that hydrous carbonated basalts can have conductivities about one magnitude higher than hydrous (CO_2-free) basalts. Thus, to achieve the most accurate determination of rheological properties of the lithosphere, geophysical methods and geochemical data of xenoliths should be applied jointly where available.

7. Conclusions

We reported infrared spectra and water contents of olivine, orthopyroxene and clinopyroxene in xenoliths from the oldest (Tihany) and youngest (Füzes-tó) alkali basalt localities of the BBHVF (central part of the CPR) for the first time. The generally low water contents of the Füzes-tó xenoliths bear resemblance to the water-poor characteristics of the NGVF xenoliths. It is suggested that both of these localities represent upper mantle portions largely affected by lithospheric thinning, which resulted in decompression and the decrease of water activity in the nominally anhydrous minerals. In contrast, the Tihany xenoliths, which have higher water contents and equilibrium temperatures compared to Füzes-tó ones likely represent the lower lithosphere which cooled and accreted during the early thermal relaxation stage after the peak extension phase. As opposed to the BBHVF and NGVF xenoliths, which are located in the central regions of the CPR, xenoliths from the marginal locations (SBVF and PMVF) have significantly higher water contents and their $D^{cpx/opx}$ values fall in a range considered 'normal' for natural

peridotites. This is because they originate from a supra-subduction environment, where the mantle is expected to be hydrated from slab-derived melts and fluids.

Calculated physical properties for the CPR xenoliths showed that xenoliths from the marginal locations with high water content have lower effective viscosities and electrical resistivities compared to those from the drier central locations. This suggests that in the central parts of extensional basins surrounded by or adjacent to subduction zones, the lithospheric mantle could be more rigid than in the margins mainly due to the decreasing water activity during decompression. Therefore, the increasing viscosity may help regain the strength of the lithosphere which can hinder further extension. However, additional factors need to be taken into account, such as differences in strain rate, which can also have a significant impact on the effective viscosity besides water content. Furthermore, the applied models ignore the potential presence of melts/fluids in the mantle, which may further decrease viscosity and resistivity if they form an interconnected network. The joint application of geochemical and geophysical (e.g., magnetotelluric) measurements can support a more accurate understanding of the lithospheric rheology.

Declaration of Competing Interest

The authors declare that they have no known competing financial interests or personal relationships that could have appeared to influence the work reported in this paper.

Acknowledgements

The authors owe thanks to Judith Mihály and Csaba Németh for their help with FTIR analyses. We are grateful for the detailed and constructive reviews of Wolfram Geissler and Ioan Seghedi, as well as for the editorial handling by Liviu Matenco. This study was financially supported by a Lendület Research Grant to the MTA CSFK Lendület Pannon LitH_2Oscope Research Group, the ELTE Institutional Excellence Program (1783-3/2018/FEKUTSRAT) by the Hungarian Ministry of Human Capacities to L. Patkó, L. E. Aradi, M. Berkesi and Cs. Szabó, the GINOP-2.3.2-15-2016-00009 research program to L. Patkó, and the Hungarian Scientific Research Fund (grant nr. NN128629, Topo-Transylvania) to I. Kovács. The manuscript is dedicated to the memory of Prof. Frank Horváth, who was a pioneer in building cooperations between geophysical and geochemical research.

This is the 103rd publication of the Lithosphere Fluid Research Lab (LRG), prepared in collaboration with the Geodetic and Geophysical Institute, Research Centre for Astronomy and Earth Sciences.

Appendix A. Supplementary data

Supplementary data to this article can be found online at https://doi.org/10.1016/j.gloplacha.2020.103364.

References

Ádám, A., Szarka, L., Novák, A., Wesztergom, V., 2017. Key results on deep electrical conductivity anomalies in the Pannonian Basin (PB), and their geodynamic aspects. Acta Geodaetica et Geophysica 52, 205–228.

Aizawa, Y., Barnhoorn, A., Faul, U.H., Fitz Gerald, J.D., Jackson, I., Kovács, I., 2008. Seismic properties of Anita Bay dunite: an exploratory study of the influence of water. J. Petrol. 49, 841–855.

Aradi, L.E., Hidas, K., Kovács, I.J., Tommasi, A., Klébesz, R., Garrido, C.J., Szabó, C., 2017. Fluid-enhanced annealing in the subcontinental lithospheric mantle beneath the westernmost margin of the Carpathian-Pannonian extensional basin system. Tectonics 36, 2987–3011.

Bada, G., Horváth, F., Dövényi, P., Szafián, P., Windhoffer, G., Cloetingh, S., 2007. Present-day stress field and tectonic inversion in the Pannonian basin. Glob. Planet. Chang. 58, 165–180.

Balázs, A., Matenco, L., Magyar, I., Horváth, F., Cloetingh, S., 2016. The link between tectonics and sedimentation in back-arc basins: New genetic constraints from the analysis of the Pannonian Basin. Tectonics 35, 1526–1559.

Balázs, A., Matenco, L., Vogt, K., Cloetingh, S., Gerya, T., 2018. Extensional Polarity Change in Continental Rifts: Inferences from 3-D Numerical Modeling and Observations. J. Geophysical Research: Solid Earth 123, 8073–8094.

Bali, E., Szabó, C., Vaselli, O., Török, K., 2002. Significance of silicate melt pockets in upper mantle xenoliths from the Bakony-Balaton Highland Volcanic Field, Western Hungary. Lithos 61, 79–102.

Bali, E., Falus, G., Szabó, C., Peate, D.W., Hidas, K., Török, K., Ntaflos, T., 2007. Remnants of boninitic melts in the upper mantle beneath the central Pannonian Basin? Mineral. Petrol. 90, 51–72.

Bali, E., Zanetti, A., Szabó, C., Peate, D.W., Waight, T.E., 2008. A micro-scale investigation of melt production and extraction in the upper mantle based on silicate melt pockets in ultramafic xenoliths from the Bakony–Balaton Highland Volcanic Field (Western Hungary). Contrib. Mineral. Petrol. 155, 165–179.

Balogh, K., Németh, K., 2005. Evidence for the neogene small-volume intracontinental. Volcanism in western Hungary: K/Ar geochronology of the Tihany Maar volcanic complex. Geol. Carpath. 56, 91–99.

Balogh, K., Árva-Sós, E., Pécskay, Z., 1986. K/Ar dating of post Sarmatian alkali basaltic rocks in Hungary. Acta Mineralogie et Petrographie Szeged 28, 75–93.

Bell, D.R., Rossman, G.R., 1992. Water in earth's mantle- the role of nominally anhydrous minerals. Science 255, 1391–1397.

Bell, D.R., Ihinger, P.D., Rossman, G.R., 1995. Quantitative analysis of trace OH in garnet and pyroxenes. Am. Mineral. 80, 465–474.

Bell, D.R., Rossman, G.R., Maldener, J., Endisch, D., Rauch, F., 2003. Hydroxide in olivine: a quantitative determination of the absolute amount and calibration of the IR spectrum. Journal of Geophysical Research: Solid Earth 1978–2012, 108. https://doi.org/10.1029/2001JB000679.

Berkesi, M., 2011. The Role of Fluids in the Lithospheric Mantle (Central Pannonian Basin, Western Hungary): Detailed Fluid Inclusion Study in Mantle Xenoliths. Eötvös Loránd University, Budapest, p. 148.

Berkesi, M., Guzmics, T., Szabó, C., Dubessy, J., Bodnar, R.J., Hidas, K., Ratter, K., 2012. The role of CO2-rich fluids in trace element transport and metasomatism in the lithospheric mantle beneath the Central Pannonian Basin, Hungary, based on fluid inclusions in mantle xenoliths. Earth Planet. Sci. Lett. 331, 8–20.

Berry, A.J., Hermann, J., O'Neill, H.S., Foran, G.J., 2005. Fingerprinting the water site in mantle olivine. Geology 33, 869–872.

Berry, A.J., O'Neill, H.S.C., Hermann, J., Scott, D.R., 2007a. The infrared signature of water associated with trivalent cations in olivine. Earth Planet. Sci. Lett. 261, 134–142.

Berry, A.J., Walker, A.M., Hermann, J., O'Neill, H.S.C., Foran, G.J., Gale, J.D., 2007b. Titanium substitution mechanisms in forsterite. Chem. Geol. 242, 176–186.

Bianchi, I., Miller, M.S., Bokelmann, G., 2014. Insights on the upper mantle beneath the Eastern Alps. Earth and Planetary Science Letters 403, 199–209.

Bielik, M., Alasonati Tašárová, Z., Vozár, J., Zeyen, H., Gutterch, A., Grad, M., Janik, T., Wybraniec, S., Götze, H., Dérerová, J., 2010. Gravity and seismic modeling in the Carpathian-Pannonian Region. In: Vozár, J., Ebner, F., Vozárová, A., Haas, J., Kovács, S., Sudar, M., Bielik, M., Péró, C. (Eds.), Variscan and Alpine Terranes of the Circum-Pannonian Region. Geological Institute, SAS, Bratislava, pp. 202–233.

Blanchard, M., Ingrin, J., Balan, E., Kovács, I.J., Withers, A.C., 2017. Effect of iron and trivalent cations on OH defects in olivine. Am. Mineral. 102, 302–311.

Brey, G.P., Köhler, T., 1990. Geothermobarometry in four-phase lherzolites II. New thermobarometers, and practical assessment of existing thermobarometers. J. Petrol. 31, 1353–1378.

Brodholt, J.P., Refson, K., 2000. An ab initio study of hydrogen in forsterite and a possible mechanism for hydrolytic weakening. Journal of Geophysical Research: Solid Earth 105, 18977–18982.

Créon, L., Rouchon, V., Youssef, S., Rosenberg, E., Delpech, G., Szabó, C., Remusat, L., Mostefaoui, S., Asimow, P.D., Antoschechkina, P., Ghiorso, M.S., Boller, E., Guyot, F., 2017. Highly CO_2-supersaturated melts in the Pannonian lithospheric mantle – A transient carbon reservoir? Lithos 286-287, 519–533.

Csontos, L., 1995. Tertiary tectonic evolution of the Intra-Carpathian area: a review. Acta Vulcanol. 7, 1–13.

Csontos, L., Nagymarosy, A., 1998. The Mid-Hungarian 824 line: a zone of repeated tectonic inversions. Tectonophysics 297 (1–4), 51–71.

Csontos, L., Nagymarosy, A., Horváth, F., Kovác, M., 1992. Tertiary evolution of the Intra-Carpathian area: a model. Tectonophysics 208, 221–241.

Dando, B.D.E., Stuart, G.W., Houseman, G.A., Hegedüs, E., Brückl, E., Radovanović, S., 2011. Teleseismic tomography of the mantle in the Carpathian–Pannonian region of Central Europe. Geophys. J. Int. 186, 11–31.

Demouchy, S., Tommasi, A., Barou, F., Mainprice, D., Cordier, P., 2012. Deformation of olivine in torsion under hydrous conditions. Phys. Earth Planet. Inter. 202-203, 56–70.

Demouchy, S., Shcheka, S., Denis, C.M., Thoraval, C., 2017. Subsolidus hydrogen partitioning between nominally anhydrous minerals in garnet-bearing peridotite. Am. Mineral. 102, 1822–1831.

Dixon, J.E., Dixon, T.H., Bell, D.R., Malservisi, R., 2004. Lateral variation in upper mantle viscosity: role of water. Earth Planet. Sci. Lett. 222, 451–467.

Embey-Isztin, A., 1976. Amphibole/lherzolite composite xenoliths from Szigliget, north of Lake Balaton, Hungary. Earth Planet. Sci. Lett. 31, 297–304.

Faccenna, C., Becker, T.W., Auer, L., Billi, A., Boschi, L., Brun, J.P., Capitanio, F.A., Funiciello, F., Horvàth, F., Jolivet, L., 2014. Mantle dynamics in the Mediterranean. Rev. Geophys. 52, 283–332.

Faccini, B., Rizzo, A.L., Bonadiman, C., Ntaflos, T., Seghedi, I., Grégoire, M., Ferretti, G., Coltorti, M., 2020. Subduction-related melt refertilisation and alkaline metasomatism in the Eastern Transylvanian Basin lithospheric mantle: Evidence from mineral chemistry and noble gases in fluid inclusions. Lithos 105516.

Falus, G., Tommasi, A., Ingrin, J., Szabó, C., 2008. Deformation and seismic anisotropy of the lithospheric mantle in the southeastern Carpathians inferred from the study of mantle xenoliths. Earth Planet. Sci. Lett. 272, 50–64.
Ferriss, E., Plank, T., Walker, D., 2016. Site-specific hydrogen diffusion rates during clinopyroxene dehydration. Contrib. Mineral. Petrol. 171, 55.
Fullea, J., 2017. On joint modelling of electrical conductivity and other geophysical and petrological observables to infer the structure of the lithosphere and underlying upper mantle. Surv. Geophys. 38, 963–1004.
Girard, J., Chen, J., Raterron, P., Holyoke, C.W., 2013. Hydrolytic weakening of olivine at mantle pressure: evidence of [100](010) slip system softening from single-crystal deformation experiments. Phys. Earth Planet. Inter. 216, 12–20.
Green, D.H., Hibberson, W.O., Kovács, I., Rosenthal, A., 2010. Water and its influence on the lithosphere-asthenosphere boundary. Nature 467, 448–451.
Harangi, S., 2001. Neogene to quaternary volcanism of the Carpathian–Pannonian Region—a review. Acta Geol. Hung. 44, 223–258.
Hirth, G., Kohlstedt, D.L., 1996. Water in the oceanic upper mantle: implications for rheology, melt extraction and the evolution of the lithosphere. Earth Planet. Sci. Lett. 144, 93–108.
Hirth, G., Kohlstedt, D., 2003. Rheology of the upper mantle and the mantle wedge: a view from the experimentalists, 138. American Geophysical Union Geophysical Monograph Series, Washington DC, pp. 83–105.
Horváth, F., Cloetingh, S., 1996. Stress-induced late-stage subsidence anomalies in the Pannonian basin. Tectonophysics 266, 287–300.
Horváth, F., 1993. Towards a mechanical model for the formation of the Pannonian basin. Tectonophysics 226, 333–357.
Horváth, F., Bada, G., Szafián, P., Tari, G., Ádám, A., Cloetingh, S., 2006. Formation and deformation of the Pannonian Basin: constraints from observational data. Geol. Soc. Lond. Mem. 32 (1), 191–206.
Houseman, G.A., Gemmer, L., 2007. Intra-orogenic extension driven by gravitational instability: Carpathian-Pannonian orogeny. Geology 35, 1135–1138.
Ismail-Zadeh, A., Matenco, L., Radulian, M., Cloetingh, S., Panza, G., 2012. Geodynamics and intermediate-depth seismicity in Vrancea (the South-Eastern Carpathians): current state-of-the art. Tectonophysics 530, 50–79.
Jankovics, É., Harangi, S., Ntaflos, T., 2009. A mineral-scale investigation of the origin of the 2.6 Ma Füzes-tó basalt, Bakony-Balaton Highland Volcanic Field (Pannonian Basin, Hungary). Cent. Eur. Geol. 52, 97–124.
Jankovics, M.É., Harangi, S., Kiss, B., Ntaflos, T., 2012. Open-system evolution of the Füzes-tó alkaline basaltic magma, western Pannonian Basin: constraints from mineral textures and compositions. Lithos 140, 25–37.
Jarosinski, M., Beekman, F., Matenco, L., Cloetingh, S., 2011. Mechanics of basin inversion: finite element modelling of the Pannonian Basin System. Tectonophysics 502, 121–145.
Jones, A.P., Smith, J.V., Dawson, J.B., Hansen, E.C., 1983. Metamorphism, partial melting, and K-metasomatism of garnet-scapolite-kyanite granulite xenoliths from Lashaine, Tanzania. J. Geol. 91, 143–165.
Jones, A.G., Evans, R.L., Eaton, D.W., 2009. Velocity–conductivity relationships for mantle mineral assemblages in Archean cratonic lithosphere based on a review of laboratory data and Hashin–Shtrikman extremal bounds. Lithos 109, 131–143.
Jones, A.G., Fullea, J., Evans, R.L., Muller, M.R., 2012. Water in cratonic lithosphere: Calibrating laboratory-determined models of electrical conductivity of mantle minerals using geophysical and petrological observations. Geochem. Geophys. Geosyst. 13, Q06010.
Jugovics, L., 1968. The set-up of the basaltic provinces of the Balaton highland and the Tapolca basin (in Hungarian). Ann. Rep. Hung. Geol. Inst. From 1968, 75–82.
Jung, H., Karato, S.-I., 2001. Water-induced fabric transitions in olivine. Science 293, 1460–1463.
Karato, S.-I., 2010. Rheology of the deep upper mantle and its implications for the preservation of the continental roots: a review. Tectonophysics 481, 82–98.
Kázmér, M., Kovács, S., 1985. Permian-Paleogene paleogeography along the eastern part of the Insubric-Periadriatic lineament system: evidence for continental escape of the Bakony-Drauzug Unit. Acta Geol. Hung. 28, 71–84.
Kovács, I., Green, D.H., Rosenthal, A., Hermann, J., O'Neill, H.S.C., Hibberson, W.O., Udvardi, B., 2012. An experimental study of water in nominally anhydrous minerals in the upper mantle near the water-saturated solidus. J. Petrol. 53, 2067–2093.
Kovács, I., Hermann, J., O'Neill, H.S.C., Gerald, J.F., Sambridge, M., Horváth, G., 2008. Quantitative absorbance spectroscopy with unpolarized light: Part II. Experimental evaluation and development of a protocol for quantitative analysis of mineral IR spectra. Am. Mineral. 93, 765–778.
Kovács, I., Falus, G., Stuart, G., Hidas, K., Szabó, C., Flower, M.F.J., Hegedűs, E., Posgay, K., Zilahi-Sebess, L., 2012a. Seismic anisotropy and deformation patterns in upper mantle xenoliths from the central Carpathian–Pannonian region: Asthenospheric flow as a driving force for Cenozoic extension and extrusion? Tectonophysics 514-517, 168–179.
Kovács, I., Lenkey, L., Green, D.H., Fancsik, T., Falus, G., Kiss, J., Orosz, L., Angyal, J., Vikor, Z., 2017. The role of pargasitic amphibole in the formation of major geophysical discontinuities in the shallow upper mantle. Acta Geodaetica et Geophysica 52, 183–204.
Kovács, I., Liptai, N., Patkó, L., Lange, T.P., Matenco, L., Cloetingh, S., Radulian, M., Molnár, G., Szakács, A., Berkesi, M., Novák, A., Wesztergom, V., Szabó, C., 2020. The 'pargasosphere' concept: or looking at global plate tectonics from a new perspective? Global and Planetary Change.
Kovács, I., Patkó, L., Falus, G., Aradi, L.E., Szanyi, G., Gráczer, Z., Szabó, C., 2018. Upper mantle xenoliths as sources of geophysical information: the Perşani Mts. Area as a case study. Acta Geodaetica et Geophysica 53, 415–438.
Kovács, I., Patkó, L., Liptai, N., Lange, T.P., Taracsák, Z., Cloetingh, S.A.P.L., Török, K., Király, E., Karátson, D., Biró, T., Kiss, J., Pálos, Z., Aradi, L.E., Falus, G., Hidas, K., Berkesi, M., Koptev, A., Novák, A., Wesztergom, V., Szabó, C., 2020. The role of water and compression in the genesis of alkaline basalts: Inferences from the Carpathian-Pannonian region. Lithos 354, 105323.
Kovács, I., Szabó, C., 2008. Middle Miocene volcanism in the vicinity of the Middle Hungarian zone: evidence for an inherited enriched mantle source. J. Geodyn. 45, 1–17.
Lange, T.P., Szabó, C., Liptai, N., Patkó, L., Gelencsér, O., Aradi, L.E., Kovács, I.J., 2019. Rheology study on the earth's mantle: Application of quantitative Fourier transform infrared spectroscopyon upper mantle xenolith from the Perşani Mountains (in Hungarian). Bull. Hung. Geol. Soc. 149, 233–254.
Laumonier, M., Farla, R., Frost, D.J., Katsura, T., Marquardt, K., Bouvier, A.-S., Baumgartner, L.P., 2017. Experimental determination of melt interconnectivity and electrical conductivity in the upper mantle. Earth Planet. Sci. Lett. 463, 286–297.
Lemaire, C., Kohn, S., Brooker, R., 2004. The effect of silica activity on the incorporation mechanisms of water in synthetic forsterite: a polarised infrared spectroscopic study. Contrib. Mineral. Petrol. 147, 48–57.
Lenkey, L., Dövényi, P., Horváth, F., Cloetingh, S., 2002. Geothermics of the Pannonian Basin and its bearing on the neotectonics. EGU Stephan Mueller Spec. Publ. Ser. 3, 29–40.
Li, Z.X.A., Lee, C.T.A., Peslier, A.H., Lenardic, A., Mackwell, S.J., 2008. Water contents in mantle xenoliths from the Colorado Plateau and vicinity: Implications for the mantle rheology and hydration-induced thinning of continental lithosphere. J. Geophys. Res. Solid Earth 1978–2012, 113. https://doi.org/10.1029/2007JB005540.
Lippitsch, R., Kissling, E., Ansorge, J., 2003. Upper mantle structure beneath the alpine orogen from high-resolution teleseismic tomography. J. Geophys. Res. Solid Earth 108.
Liptai, N., Patkó, L., Kovács, I.J., Hidas, K., Pintér, Z., Jeffries, T., Zajacz, Z., O'Reilly, S. Y., Griffin, W.L., Pearson, N.J., Szabó, C., 2017. Multiple metasomatism beneath the Nógrád–Gömör Volcanic Field (Northern Pannonian Basin) revealed by upper mantle peridotite xenoliths. J. Petrol. 58, 1107–1144.
Liptai, N., Hidas, K., Tommasi, A., Patkó, L., Kovács, I.J., Griffin, W.L., O'Reilly, S.Y., Pearson, N.J., Szabó, C., 2019. Lateral and Vertical Heterogeneity in the Lithospheric Mantle at the Northern margin of the Pannonian Basin Reconstructed from Peridotite Xenolith Microstructures. J.Geophys. Res. Solid Earth 124, 6315–6336.
Lloyd, A.S., Ferriss, E., Ruprecht, P., Hauri, E.H., Jicha, B.R., Plank, T., 2016. An assessment of clinopyroxene as a recorder of magmatic water and magma ascent rate. J. Petrol. 57, 1865–1886.
Mackwell, S., Kohlstedt, D., Paterson, M., 1985. The role of water in the deformation of olivine single crystals. J. Geophys. Res. Solid Earth 90, 11319–11333.
Manthilake, M., Miyajima, N., Heidelbach, F., Soustelle, V., Frost, D., 2013. The effect of aluminum and water on the development of deformation fabrics of orthopyroxene. Contrib. Mineral. Petrol. 165, 495–505.
Martin, R., Donnay, G., 1972. Hydroxyl in the mantle. Am. Mineral. J. Earth Planet. Mater. 57, 554–570.
Mei, S., Kohlstedt, D., 2000. Influence of water on plastic deformation of olivine aggregates: 2. Dislocation creep regime. J. Geophys. Res. Solid Earth 105, 21471–21481.
Miller, K.J., Montési, L.G.J., Zhu, W.-L., 2015. Estimates of olivine–basaltic melt electrical conductivity using a digital rock physics approach. Earth Planet. Sci. Lett. 432, 332–341.
Mitterbauer, U., Behm, M., Brückl, E., Lippitsch, R., Guterch, A., Keller, G.R., Koslovskaya, E., Rumpfhuber, E.-M., Šumanovac, F., 2011. Shape and origin of the East-Alpine slab constrained by the ALPASS teleseismic model. Tectonophysics 510, 195–206.
Nemcok, M., Pospisil, L., Lexa, J., Donelick, R.A., 1998. Tertiary subduction and slab break-off model of the Carpathian–Pannonian region. Tectonophysics 295, 307–340.
Ni, H., Keppler, H., Behrens, H., 2011. Electrical conductivity of hydrous basaltic melts: implications for partial melting in the upper mantle. Contrib. Mineral. Petrol. 162, 637–650.
Nimis, P., Grütter, H., 2010. Internally consistent geothermometers for garnet peridotites and pyroxenites. Contrib. Mineral. Petrol. 159, 411–427.
Novella, D., Jacobsen, B., Weber, P.K., Tyburczy, J.A., Ryerson, F.J., Du Frane, W.L., 2017. Hydrogen self-diffusion in single crystal olivine and electrical conductivity of the Earth's mantle. Sci. Rep. 7, 1–10.
Patkó, L., Liptai, N., Kovács, I.J., Aradi, L.E., Xia, Q.-K., Ingrin, J., Mihály, J., O'Reilly, S. Y., Griffin, W.L., Wesztergom, V., Szabó, C., 2019. Extremely low structural hydroxyl contents in upper mantle xenoliths from the Nógrád-Gömör Volcanic Field (northern Pannonian Basin): Geodynamic implications and the role of post-eruptive re-equilibration. Chem. Geol. 507, 23–41.
Patkó, L., Créon, L., Kovács, Z., Liptai, N., Rosenberg, E., Szabó, C., 2020b. Three-dimensional distribution of glass and vesicles in metasomatized xenoliths: a micro-CT case study from Nógrád-Gömör Volcanic Field (Northern Pannonian Basin). Geol. Carpath. 71, 418–423.
Patkó, L., Liptai, N., Aradi, L.E., Klébesz, R., Sendula, E., Bodnar, R.J., Kovács, I.J., Hidas, K., Cesare, B., Novák, A., Trásy, B., Szabó, C., 2020a. Metasomatism-induced wehrlite formation in the upper mantle beneath the Nógrád-Gömör Volcanic Field (Northern Pannonian Basin): evidence from xenoliths. Geosci. Front. 11, 934–364.
Patkó, L., Novák, A., Klébesz, R., Liptai, N., Lange, T.P., Molnár, G., Csontos, L., Wesztergom, V., Kovács, I.J., Szabó, C., 2020. Effect of metasomatism on the electrical resistivity of the lithospheric mantle - an integrated research using magnetotelluric sounding and xenoliths beneath the Nógrád-Gömör Volcanic Field. Global and Planetary Change.
Pécskay, Z., Lexa, J.A.S., Balogh, K., Seghedi, I., Konečny, V., Kovács, M., Márton, E., Kaliciak, M., Széky-Fux, V., Póka, T., Gyarmati, P., Edelstein, O., Rosu, E., Zec, B., 1995. Space and time distribution of Neogene-Quartenary volcanism in the Carpatho-Pannonian Region. Acta Vulcanol. 7, 15–28.

Peslier, A.H., 2010. A review of water contents of nominally anhydrous natural minerals in the mantles of Earth, Mars and the Moon. J. Volcanol. Geotherm. Res. 197, 239–258.
Peslier, A.H., Schönbächler, M., Busemann, H., Karato, S.-I., 2017. Water in the Earth's Interior: distribution and Origin. Space Sci. Rev. 212, 743–810.
Poe, B.T., Romano, C., Nestola, F., Smyth, J.R., 2010. Electrical conductivity anisotropy of dry and hydrous olivine at 8 GPa. Phys. Earth Planet. Inter. 181, 103–111.
Qorbani, E., Bianchi, I., Bokelmann, G., 2015. Slab detachment under the Eastern Alps seen by seismic anisotropy. Earth Planet. Sci. Lett. 409, 96–108.
Ratschbacher, L., Frisch, W., Linzer, H.G., Merle, O., 1991. Lateral extrusion in the Eastern Alps, part 2: structural analysis. Tectonics 10, 257–271.
Royden, L.H., Horváth, F., Burchfiel, B.C., 1982. Transform faulting, extension and subduction in the Carpathian-Pannonian region. Geol. Soc. Am. Bull. 93, 717–725.
Royden, L., Horváth, F., Rumpler, J., 1983. Evolution of the Pannonian Basin System: 1. Tectonics. Tectonics 2, 63–90.
Sambridge, M., Gerald, J.F., Kovács, I., O'Neill, H.S.C., Hermann, J., 2008. Quantitative absorbance spectroscopy with unpolarized light: part I. Physical and mathematical development. Am. Mineral. 93, 751–764.
Seghedi, I., Downes, H., 2011. Geochemistry and tectonic development of Cenozoic magmatism in the Carpathian–Pannonian region. Gondwana Res. 20, 655–672.
Seghedi, I., Downes, H., Szakács, A., Mason, P.R.D., Thirlwall, M.F., Roşu, E., Pécskay, Z., Márton, E., Panaiotu, C., 2004. Neogene–Quaternary magmatism and geodynamics in the Carpathian–Pannonian region: a synthesis. Lithos 72, 117–146.
Selway, K., 2014. On the causes of electrical conductivity anomalies in tectonically stable lithosphere. Surv. Geophys. 35, 219–257.
Selway, K., Yi, J., Karato, S.-I., 2014. Water content of the Tanzanian lithosphere from magnetotelluric data: Implications for cratonic growth and stability. Earth Planet. Sci. Lett. 388, 175–186.
Sifré, D., Gardés, E., Massuyeau, M., Hashim, L., Hier-Majumder, S., Gaillard, F., 2014. Electrical conductivity during incipient melting in the oceanic low-velocity zone. Nature 509, 81–85.
Stalder, R., Skogby, H., 2003. Hydrogen diffusion in natural and synthetic orthopyroxene. Phys. Chem. Miner. 30, 12–19.
Szabó, C., Harangi, S., Csontos, L., 1992. Review of Neogene and Quaternary volcanism of the Carpathian-Pannonian region. Tectonophysics 208, 243–256.
Szabó, C., Bodnar, R.J., Sobolev, A.V., 1996. Metasomatism associated with subduction-related, volatile-rich silicate melt in the upper mantle beneath the Nograd-Gomor volcanic field, northern Hungary/southern Slovakia; evidence from silicate melt inclusions. Eur. J. Mineral. 8, 881–899.
Szabó, C., Falus, G., Zajacz, Z., Kovács, I., Bali, E., 2004. Composition and evolution of lithosphere beneath the Carpathian–Pannonian Region: a review. Tectonophysics 393, 119–137.
Szabó, C., Hidas, K., Bali, E., Zajacz, Z., Kovács, I., Yang, K., Guzmics, T., Török, K., 2009. Melt-wall rock interaction in the mantle shown by silicate melt inclusions in peridotite xenoliths from the central Pannonian Basin (western Hungary). Island Arc 18, 375–400.
Szafián, P., Horváth, F., 2006. Crustal structure in the Carpatho-Pannonian region: insights from three-dimensional gravity modelling and their geodynamic significance. Int. J. Earth Sci. 95, 50–67.
Tašárová, A., Afonso, J.C., Bielik, M., Götze, H.J., Hók, J., 2009. The lithospheric structure of the Western Carpathian–Pannonian Basin region based on the CELEBRATION 2000 seismic experiment and gravity modelling. Tectonophysics 475, 454–469.
Tian, Z.-Z., Liu, J., Xia, Q.-K., Ingrin, J., Hao, Y.-T., Christophe, D., 2017. Water concentration profiles in natural mantle orthopyroxenes: a geochronometer for long annealing of xenoliths within magma. Geology 45, 87–90.
Tielke, J.A., Zimmerman, M.E., Kohlstedt, D.L., 2017. Hydrolytic weakening in olivine single crystals. J. Geophys. Res. Solid Earth 122, 3465–3479.
Tondi, R., Achauer, U., Landes, M., Daví, R., Besutiu, L., 2009. Unveiling seismic and density structure beneath the vrancea seismogenic zone, Romania. J. Geophys. Res. Solid Earth 114.
Walker, A., Hermann, J., Berry, A.J., O'Neill, H.S.C., 2007. Three water sites in upper mantle olivine and the role of titanium in the water weakening mechanism. J. Geophys. Res. Solid Earth 112.
Wallace, M., Green, D., 1991. The effect of bulk rock composition on the stability of amphibole in the upper mantle: implications for solidus positions and mantle metasomatism. Mineral. Petrol. 44, 1–19.
Wang, D., Mookherjee, M., Xu, Y., Karato, S.-I., 2006. The effect of water on the electrical conductivity of olivine. Nature 443, 977–980.
Warren, J.M., Hirth, G., 2006. Grain size sensitive deformation mechanisms in naturally deformed peridotites. Earth Planet. Sci. Lett. 248, 438–450.
Wijbrans, J., Németh, K., Martin, U., Balogh, K., 2007. 40Ar/39Ar geochronology of Neogene phreatomagmatic volcanism in the western Pannonian Basin, Hungary. J. Volcanol. Geotherm. Res. 164, 193–204.
Xia, Q.-K., Liu, J., Liu, S.-C., Kovács, I., Feng, M., Dang, L., 2013. High water content in Mesozoic primitive basalts of the North China Craton and implications on the destruction of cratonic mantle lithosphere. Earth Planet. Sci. Lett. 361, 85–97.
Xia, Q.-K., Liu, J., Kovács, I., Hao, Y.-T., Li, P., Yang, X.-Z., Chen, H., Sheng, Y.-M., 2019. Water in the upper mantle and deep crust of eastern China: concentration, distribution and implications. Natl. Sci. Rev. 6, 125–144.
Yoshino, T., Matsuzaki, T., Shatskiy, A., Katsura, T., 2009. The effect of water on the electrical conductivity of olivine aggregates and its implications for the electrical structure of the upper mantle. Earth Planet. Sci. Lett. 288, 291–300.